

Investigation of Total Collision Energy and Underlying Event Activity via Transverse Energy
Measurements in Au+Au and p+p collisions at 200 GeV with the sPHENIX Detector

Emma McLaughlin

Submitted in partial fulfillment of the
requirements for the degree of
Doctor of Philosophy
under the Executive Committee
of the Graduate School of Arts and Sciences

COLUMBIA UNIVERSITY

2025

© 2025

Emma McLaughlin

All Rights Reserved

Abstract

Investigation of Total Collision Energy and Underlying Event Activity via Transverse Energy

Measurements in Au+Au and p+p collisions at 200 GeV with the sPHENIX Detector

Emma McLaughlin

problem of the thesis/dissertation, (2) discuss the materials and methods used, and (3) state the conclusions reached. Individual chapters should not have abstracts.

Table of Contents

Acknowledgments	vi
Dedication	vii
Introduction or Preface	1
Chapter 1: Introduction and Background	2
1.1 Footnotes: Two ways of adding to your text	2
1.2 Other section of first chapter	2
Chapter 2: Experimental Detector Design	3
2.1 Relativistic Heavy Ion Collider	3
2.2 sPHENIX Detector	3
2.2.1 sPHENIX Tracking System	4
2.2.2 sPHENIX Calorimeter System	11
2.2.3 sPHENIX Global Detectors	13
2.2.4 sPHENIX Data Acquisition and Readout	16
Chapter 3: sPHENIX Calorimeter Commissioning, Reconstruction and Calibration	20
3.1 Real-time Calorimeter State Logging and Monitoring	20
3.2 sPHENIX Low-Level Data Reconstruction	23

3.2.1	Diagnosing ADC Bit Issues	23
3.2.2	Online ADC Firmware Fixes	23
3.2.3	Offline Reconstruction Software Fixes	23
3.3	sPHENIX Calorimeter Calibration and Reconstruction Routines	27
3.3.1	Calorimeter Tower Reconstruction	27
3.3.2	EMCal Energy Calibration	27
3.3.3	HCal Energy Calibration	27
	Chapter 4: Transverse Energy Density Measurements in Au+Au Collisions	28
	Chapter 5: Underlying Event Measurements in p+p Collisions	29
	Chapter 6: Last Chapter before conclusion	30
	Conclusion or Epilogue	31
	References	32
	Appendix A: Experimental Equipment	34
	Appendix B: Data Processing	35

List of Figures

2.1	Diagram of full array of sPHENIX physics program goals including measurements in jet structure, heavy flavor, quarkonia, bulk heavy ion physics and proton spin physics.	4
2.2	sPHENIX detector with subsystems labeled.	5
2.3	(a) Schematic of an sPHENIX MVTX stave (left) and half barrel layer made up of staves and service section (right). (b) Cross-section of MVTX silicon barrel with its 3 layers highlighted in different colors (Red, Green, and Blue) and sPHENIX beam pipe included to highlight the MVTX location relative to the beam pipe. Reproduced from [1].	7
2.4	Schematic of sPHENIX INTT silicon ladder component. Highlighted on silicon ladder are silicon sensors, readout chips and high-density interconnect (HDI) cables. Reproduced from [4].	8
2.5	Left: Cross-section schematic of sPHENIX TPC showing central membrane (CM), inner- and outer-field cages (I-FC, O-FC) and end plates (EP). Middle: Segmentation of TPC endcap into 72 GEM modules. Right: Schematic of TPC GEM modules highlighting the four foil layers with varying electric fields and pad plane for readout of amplified signal. Reproduced from [5].	9
2.6	(a) Schematic of sPHENIX TPOT detector (left). (b) Schematic of track reconstruction using all tracking subsystems highlighting the benefit to having a TPOT hit for drift corrections. (c) Cross-section of TPOT Micromegas chamber. Reproduced from [7].	10
2.7	(a) Photo of the sPHENIX EMCal, IHCAL and OHCal detectors after installation and cabling. (b) Graphic of sPHENIX IHCAL (red), OHCal (gray) and superconducting magnet (pink) from GEANT simulation. IHCAL(OHCal) scintillator tiles shown in yellow(green).	11
2.8	(a) Schematic of EMCal sector highlighting projective geometry of towers in η and lightguides and electronics on the inner radius of the sector. (b) Schematic of OHCal half-sector highlighting projective geometry of towers in η , layered absorber/scintillator tile tower design, wavelength-shifting fiber located within HCal scintillating tiles, and readout electronics on the outer radius of the sector. Reproduced from [5].	12
2.9	Left: Schematic of 64 MBD module array mounted on detector frame. Right: Photo of individual MBD module with quartz radiator and PMT. Reproduced from [5].	14

2.10 Schematic of sPHENIX ZDC detector shown from (a) collision region view and (b) "beam's eye" view to show the ZDC location past the RHIC DX dipole magnets and between the beam pipes. Also shown is the trajectory of beam fragments with neutrons measured in the region of the ZDC and protons deflected. Reproduced from [12].	15
2.11 Flowchart of sPHENIX data aquisition system showing progagation through the stages of data aquisition from the front end electronics to the RHIC computing facility. Reproduced from [5].	17
2.12 Detailed flowchart of sPHENIX data aquisition system for triggered subsystems (calorimeters and global detectors) including feedback on data readout from Trigger System. Reproduced from [5].	18
3.1 (a) Diagram of EMCal sector design with interface board connections to slow control, MPOD, low voltage power and ADC boards. (b) Diagram of HCal half-sector design with interface board connections to slow control, MPOD, low voltage power and ADC boards. Reproduced from [5]	21
3.2 Diagram of HCal database table schema for logging detector state information. Includes tables for hcal slow control and bias voltage information as well as LED and pedestal run analysis results.	22
3.3 (a) Shifter monitoring dashboard for HCal gain, SiPM temperature and bias voltage offsets, LED and Pin Diode status. (b) Bias voltage monitoring dashboard showing the bias voltage for sector of the HCal.	24
3.4 Diagram of the ADC board design used for digitization of signals from the sPHENIX calorimeters.	25
3.5 Pseudo-code algorithm for discovering and recovering calorimeter waveforms digi- tized with stuck high value bits using the quality of fit to the calorimeter waveform template.	26
3.6 Example waveforms of before (left) and after (right) the waveform recovery method for an EMCal channel with a known intermittent stuck bit.	26

List of Tables

1.1 This is an example Table.	2
---------------------------------------	---

Acknowledgements

Insert your acknowledgements text here. This page is optional, you may delete it if not needed.

Dedication

Insert your dedication text here. This page is optional, you may delete it if not needed.

Introduction or Preface

Insert your preface text here if applicable. This page is optional, you may delete it if not needed. If you delete this page make sure to move page counter comment in thesis.tex to correct location.

Chapter 1: Introduction and Background

1.1 Footnotes: Two ways of adding to your text

¹. Or it is possible to mark the location of a foot note with footnote mark command² then you can write the footnote in its own line for ease of reading.

1.2 Other section of first chapter

¹By using footnote command and writing your note in the curly brackets

²You then use footnotetext command and then write you note in as if you are using regular footnote command as we did previously.

Table 1.1: This is an example Table.

x	f(x)	g(x)
1	6	4
2	6	3
3	6	2
4	6	2

Chapter 2: Experimental Detector Design

2.1 Relativistic Heavy Ion Collider

2.2 sPHENIX Detector

The super Pioneering High Energy Nuclear Interaction eXperiment (sPHENIX) detector is located at RHIC and employs an array of central tracking, calorimeter and global event characterization subsystems in order to make measurements of the heavy ion and proton-proton collisions that occur from the RHIC beams. sPHENIX is the first general purpose detector to be built on a particle collider in the last decade and has been built with specific goals of measuring jets, heavy flavor and quarkonia at RHIC energies for direct comparison with measurements in the last decade from the LHC experiments. The full array of sPHENIX physics program goals can be found in Fig. 2.1.

sPHENIX began data taking in 2023 with a commissioning dataset of Au+Au collisions at $\sqrt{s_{NN}} = 200$ GeV. In 2024, sPHENIX took its premire physics dataset of p+p collisions at $\sqrt{s} = 200$ GeV sampling over 100 pb^{-1} allowing for precision jet measurements in p+p collisions at RHIC energies. sPHENIX also collected an additional dataset of Au+Au collisions at $\sqrt{s_{NN}} = 200$ GeV in 2024 intended for the commissioning of the tracking detectors with the calorimeter system and global detectors in full physics datataking mode. This Au+Au dataset was very useful in validating the calorimeter and jet reconstruction, calibration and preformance and provided confidence in the sPHENIX data collection and reconstruction prior to the sPHENIX high statistics flagship Au+Au dataset collected in 2025 sampling 7 nb^{-1} . The results shown in this thesis are from the 2024 p+p and Au+Au datasets.

sPHENIX has three main subsystem groups: a 4-part tracking system with a MAPS-based vertex detector (MVTX), an intermediate silicon tracker (INTT), the time projection chamber (TPC)

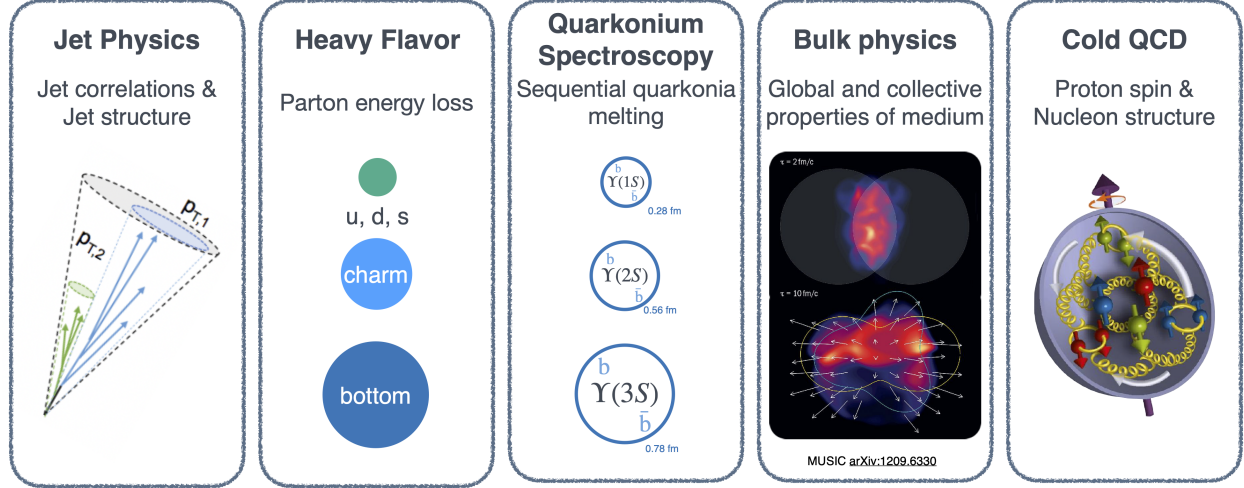


Figure 2.1: Diagram of full array of sPHENIX physics program goals including measurements in jet structure, heavy flavor, quarkonia, bulk heavy ion physics and proton spin physics.

and the TPC Outer Tracker (TPOT), a central barrel calorimeter system with three calorimeter layers of electromagnetic and hadronic calorimetry (EMCal, IHCal and OHCal), and global detectors including the Minimum Bias Detector (MBD), Zero Degree Calorimeters (ZDCs) and sPHENIX Event Plane Detector (sEPD). A rendering of the sPHENIX detector highlighting these subsystems with labels can be found in Fig. 2.2.

2.2.1 sPHENIX Tracking System

The sPHENIX tracking system comprises four subdetectors: a MAPS-based vertex detector (MVTX), an intermediate silicon tracker (INTT), the time projection chamber (TPC) and the TPC Outer Tracker (TPOT). These tracking subdetectors can provide a combination of particle momentum measurements, particle species identification, and secondary vertex reconstruction for use in physics measurements especially related to heavy flavor physics and jet substructure.

The MVTX is the innermost tracking subsystem, at a distance of 2-5 cm from the beam pipe, and is a 3 layer silicon barrel design with full azimuthal coverage ($0 < \phi < 2\pi$) and pseudorapidity coverage of $|\eta| < 1$. Each layer of silicon barrel is composed of a set of staves, for a total of 48 staves, which each contain a hybrid integrated circuit with a flexible printed circuit connected to nine ALICE Pixel Detector (ALPIDE) pixel chip sensors, for a total of 432 ALPIDE sensors [1,

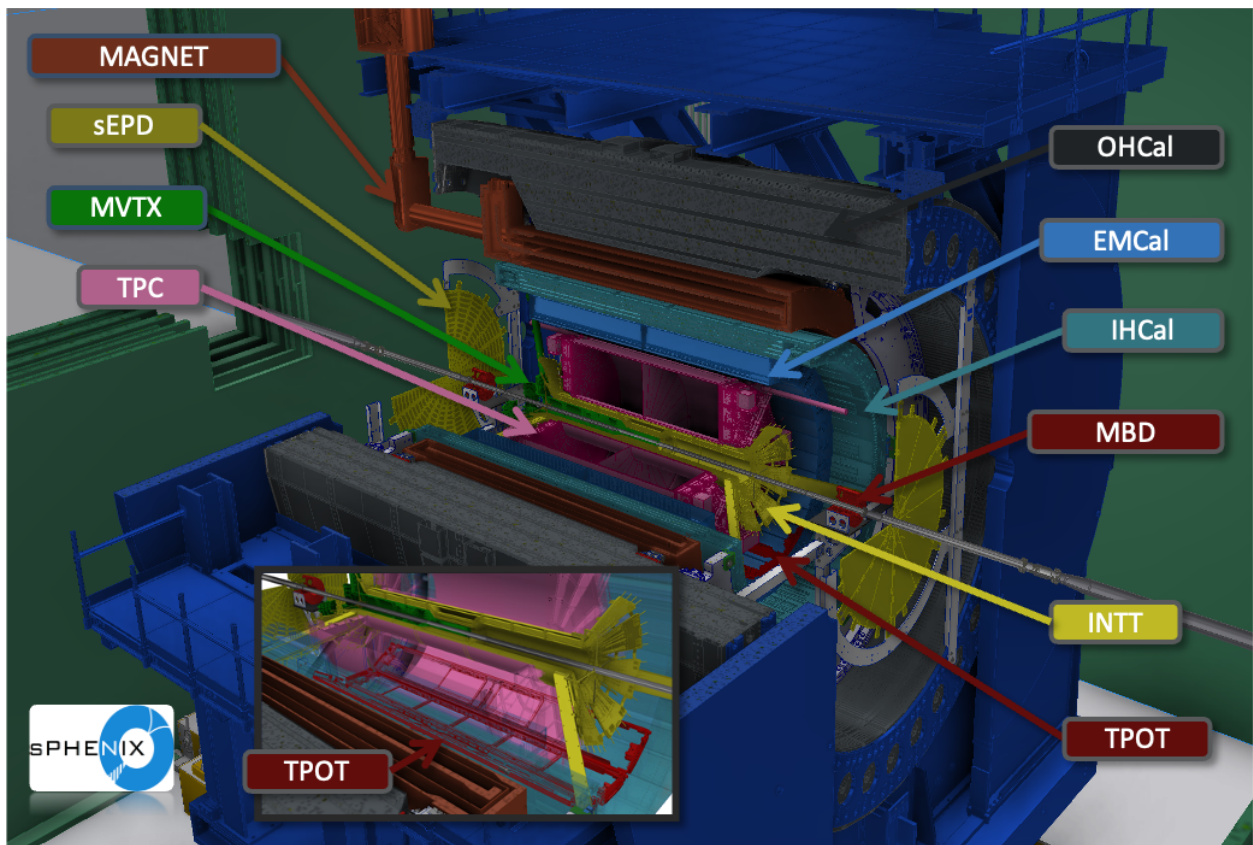
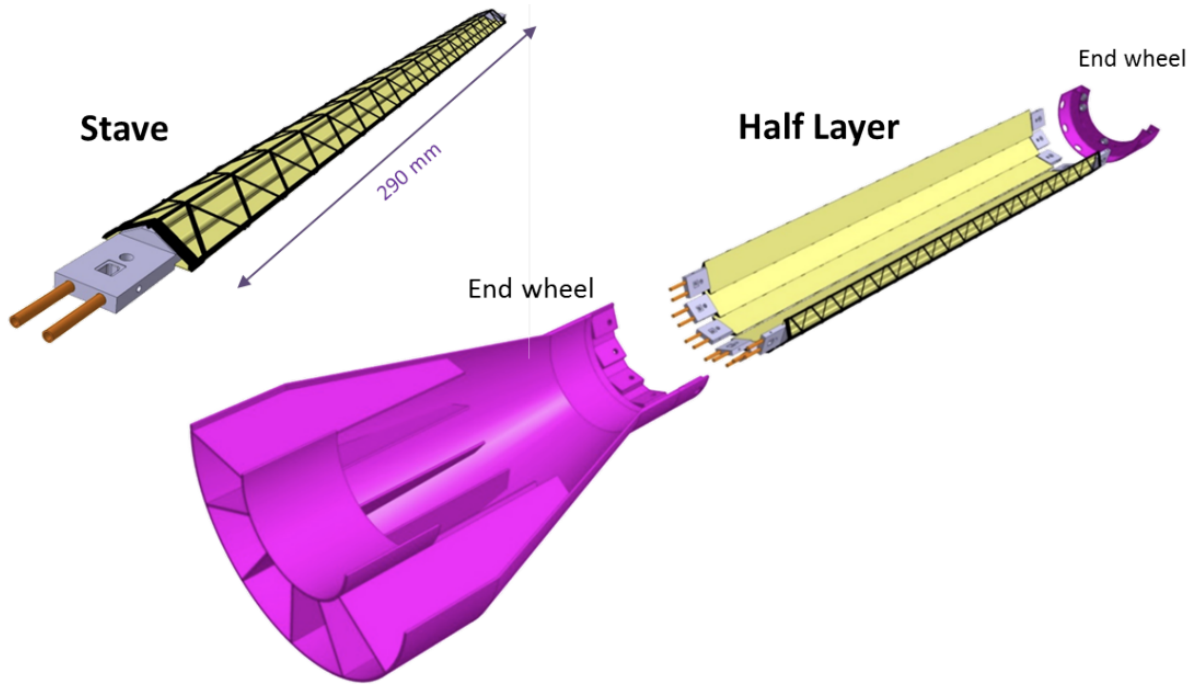


Figure 2.2: sPHENIX detector with subsystems labeled.

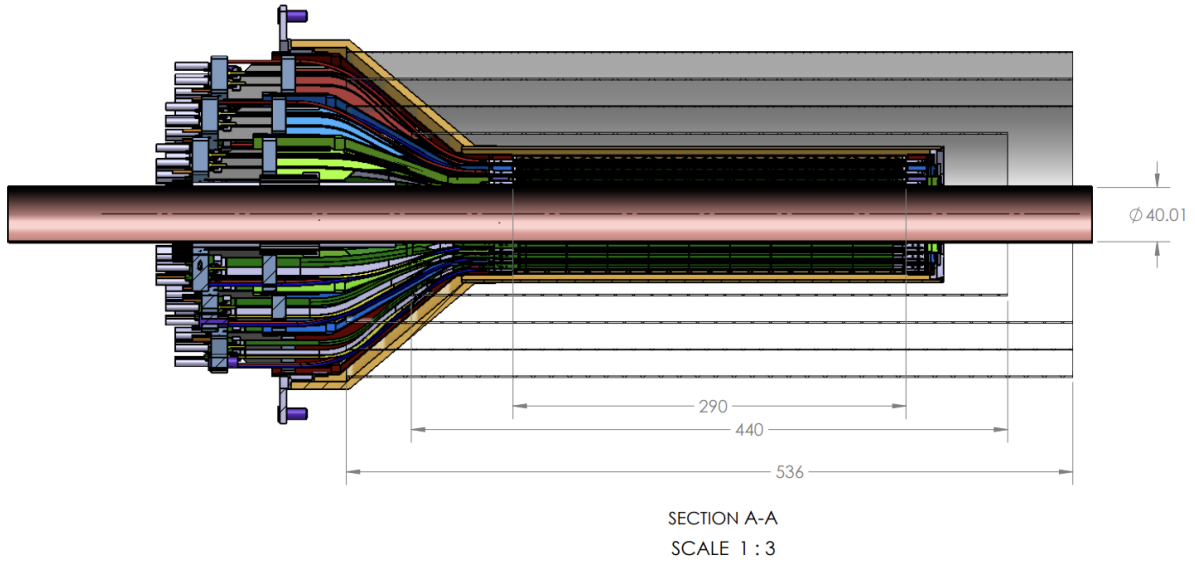
2]. The ALPIDE sensors are Monolithic Active Pixel Sensors (MAPS) that use Complementary Metal Oxide Semiconductor (CMOS) technology to build the pixel directly on the read out chip. The sensor consists of a silicon die of size 15 mm x 30 mm with an active p-doped epitaxial layer where charge is freed by an incoming particle and a set of charge collection diodes (pixels) with position resolution of 30 μm where the charge is then collected. Following collection, the sensors also amplify and digitize signals from each pixel and zero suppression is applied before read out. The MVTX is essential in sPHENIX’s ability to make heavy flavor measurements [3]. By utilizing its high precision position resolution and streaming readout capabilities, the MVTX can reconstruct a large sample of decay vertices from heavy flavor hadrons.

The INTT is a two-layer silicon barrel subsystem located between the MVTX and TPC with the first layer at a radial distance of 7.5 cm and second layer at 10 cm and has full azimuthal coverage, which is ensured by staggering the silicon sensors of the two layers in ϕ . The INTT barrels are composed of silicon ladders containing silicon strip sensors, readout chips, high-density interconnect cables and a carbon fiber stave that serves as a support structure [4]. At the silicon sensor, electron-hole pairs are created when charge particles pass through the detector. This signal is then digitized, zero suppression is applied and the data is read out via the high-density interconnect cables to readout cards. INTT hits can be used to bridge the MVTX and TPC tracks to improve tracking reconstruction. However, the INTT is also essential in associating reconstructed tracks with data from the sPHENIX calorimeter system and global detectors which are readout in triggered mode. This is done by using the precise timing resolution of the INTT hits, therefore reconstructed tracks can be associated with RHIC bunch crossings by using the timing of their INTT hits [4].

The TPC is the main sPHENIX tracking subdetector, spanning in radial distance from 20 to 80 cm with full azimuthal coverage ($0 < \phi < 2\pi$) and pseudorapidity coverage of $|\eta| < 1.1$. The sPHENIX TPC is a cylindrical double-sided TPC design with a central membrane at the center of the detector and two readout endcaps on the interior of either side of the detector’s span in z. In each half of the TPC, an electric field is formed by setting the central membrane electrode to



(a) MVTX stave and half-barrel layer



(b) MVTX detector barrel

Figure 2.3: (a) Schematic of an sPHENIX MVTX stave (left) and half barrel layer made up of staves and service section (right). (b) Cross-section of MVTX silicon barrel with its 3 layers highlighted in different colors (Red, Green, and Blue) and sPHENIX beam pipe included to highlight the MVTX location relative to the beam pipe. Reproduced from [1].

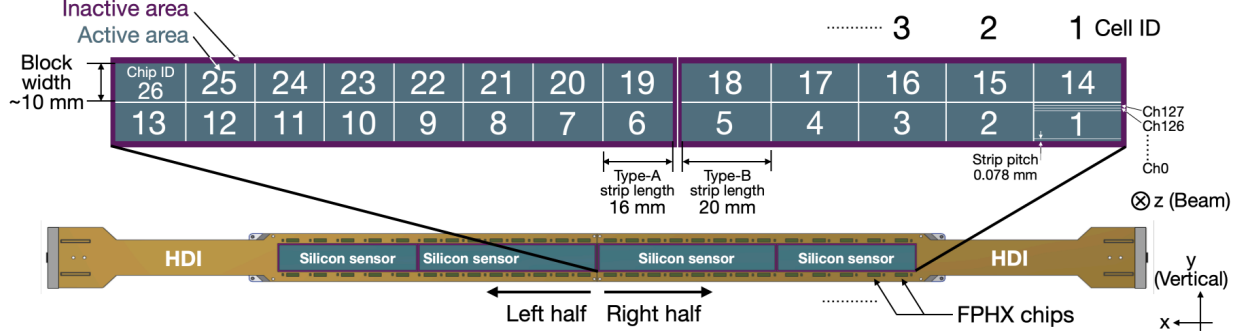


Figure 2.4: Schematic of sPHENIX INTT silicon ladder component. Highlighted on silicon ladder are silicon sensors, readout chips and high-density interconnect (HDI) cables. Reproduced from [4].

a high voltage and the readout endcaps to ground [5, 6]. This electric field is constrained in the radial direction by field cages on the inner and outer cylindrical surfaces of the TPC. The TPC volume is also filled with a gas mixture of Argon, CF₄ and Isobutane in a ratio of 75:20:5. When charged particles from the collision pass through the TPC gas volume, they ionize the gas creating electrons and ions, which act as signal for use in determining particle trajectories through the TPC. These freed electrons then drift towards the readout endcaps via the electric field between the central membrane and the readout endcaps.

On each end of the TPC there is an amplification region where Gaseous Electron Multipliers (GEM) modules are used to amplify the signal from ionized electrons within the TPC volume. Each GEM module contains a stack of four Kapton + Copper foils with a varying voltage across each foil creating a high electric field within the holes of the foils. As electrons pass through the full GEM stack they undergo avalanche amplification, where each foil contributes a small amount of the overall electron amplification. The electric fields between the GEM foils are also able to minimize the amount of avalanche induced positive ions that drift back into the TPC volume thereby reducing ion back flow and allowing the TPC to operate continuous readout. Finally the amplified electron signals are read out using SAMPA chips developed by ALICE each which contain 32 channels. The TPC has a total of 159,744 readout channels read out through a set of 6, 8 and 12 Front End Electronics (FEE) corresponding to the inner (R1), middle (R2) and outer (R3) radial regions of

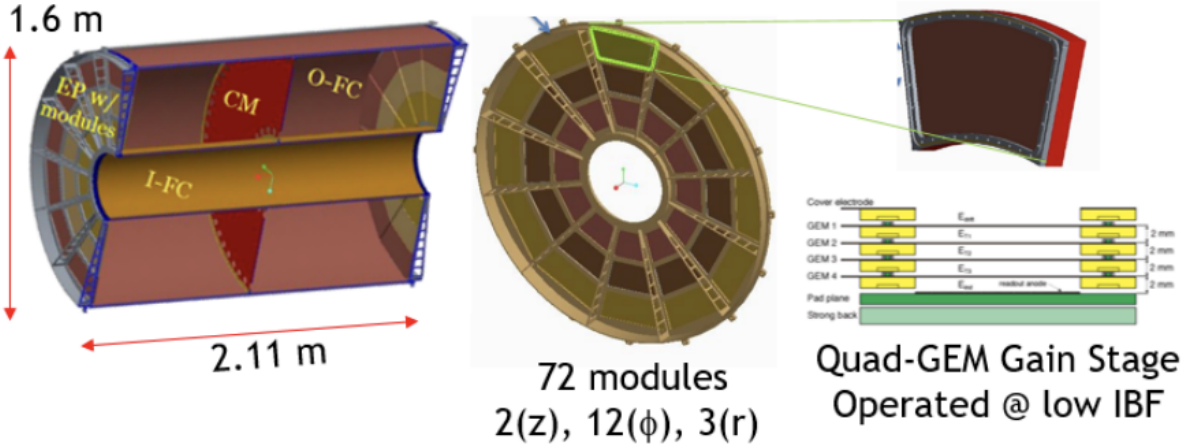


Figure 2.5: Left: Cross-section schematic of sPHENIX TPC showing central membrane (CM), inner- and outer-field cages (I-FC, O-FC) and end plates (EP). Middle: Segmentation of TPC endcap into 72 GEM modules. Right: Schematic of TPC GEM modules highlighting the four foil layers with varying electric fields and pad plane for readout of amplified signal. Reproduced from [5].

the TPC endcaps.

The TPOT is a Micromegas-based detector located just outside the TPC outer cylinder and used for facilitating in-situ TPC calibration by measuring real time distortions in the electron drift within the TPC [7]. The TPOT covers a total of 8% of the TPC acceptance and comprises four modules which cover the full z range of the bottom-most TPC sector and four addition modules, split between the two neighboring TPC sectors in ϕ . Each module contains two radially stacked Micromegas chambers where the first chamber measures the z coordinate and the second measures the ϕ coordinate of a transversing particle. Each Micromegas chamber contains a drift electrode, a micromesh, a resistive layer and a readout layer with an electric field applied across the layers to guide ionization electrons through the drift gap. The micromesh separates the ionization electron drift and amplification regions and the readout layer collects signals which are then read out via a set of front end electronics (FEEs).

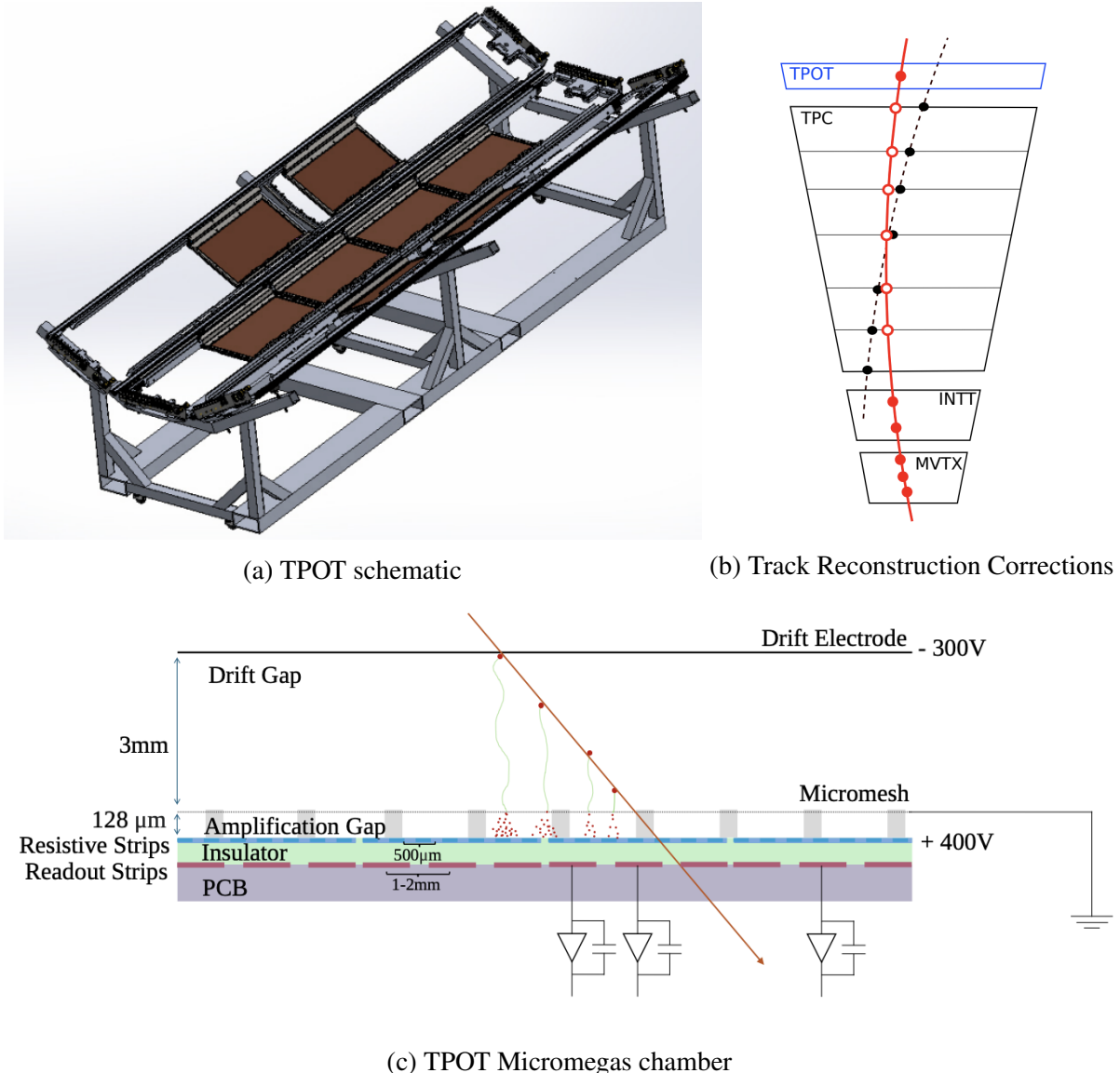
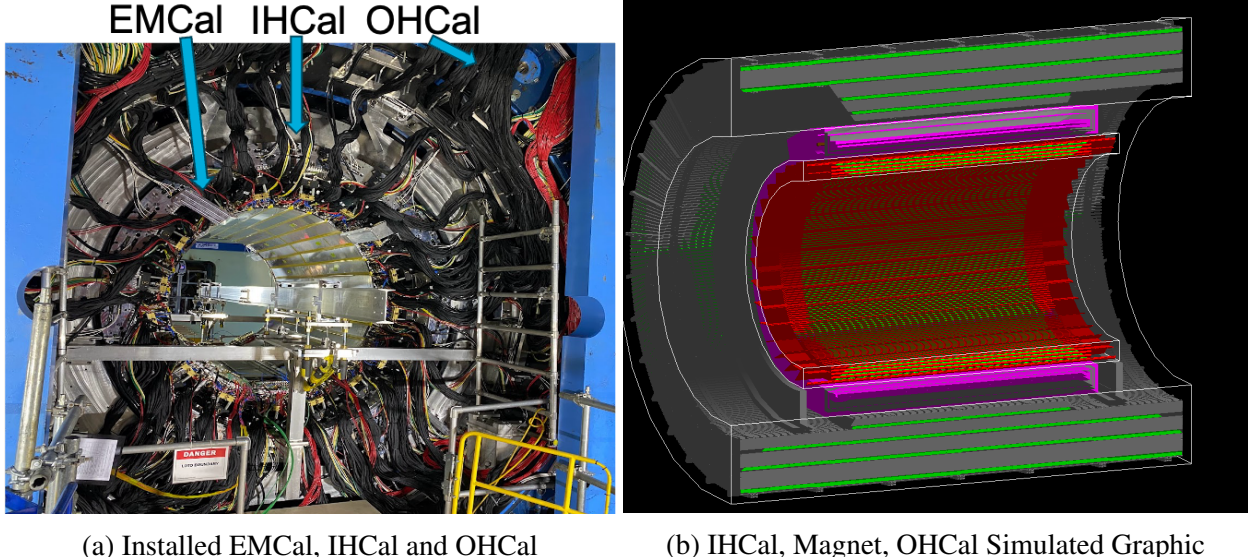


Figure 2.6: (a) Schematic of sPHENIX TPOT detector (left). (b) Schematic of track reconstruction using all tracking subsystems highlighting the benefit to having a TPOT hit for drift corrections. (c) Cross-section of TPOT Micromegas chamber. Reproduced from [7].



(a) Installed EMCAL, IHCal and OHCal

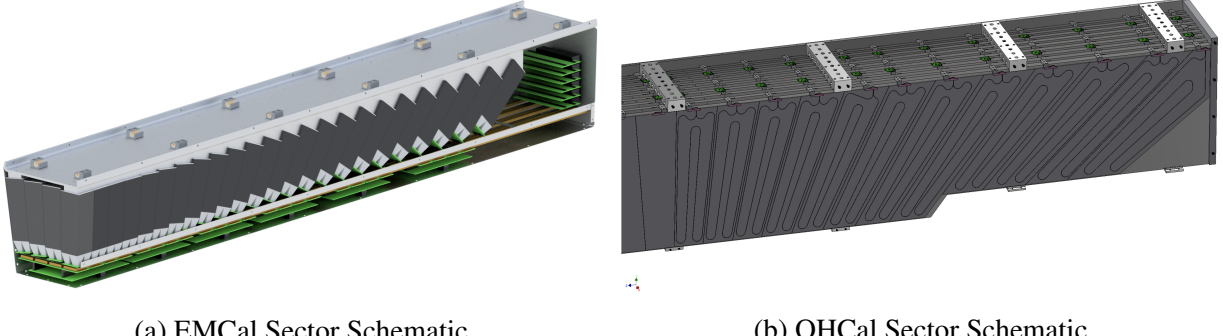
(b) IHCal, Magnet, OHCal Simulated Graphic

Figure 2.7: (a) Photo of the sPHENIX EMCAL, IHCal and OHCal detectors after installation and cabling. (b) Graphic of sPHENIX IHCal (red), OHCal (gray) and superconducting magnet (pink) from GEANT simulation. IHCal(OHCal) scintillator tiles shown in yellow(green).

2.2.2 sPHENIX Calorimeter System

sPHENIX has three central barrel calorimeter layers, an electromagnetic calorimeter (EMCal), an inner hadronic calorimeter (IHCal) and an outer hadronic calorimeter (OHCal). These calorimeter subdetectors provide energy measurements of all particles, both neutral and charged, for use online in triggering on rare physics probes like high momentum photons and jets and offline for use mainly in jet measurements. These detectors are concentric and sandwich the sPHENIX magnet with the EMCal located closest to the interaction point and the OHCal located further from the interaction point within the calorimeter system. Further, these detectors have full azimuthal coverage ($0 < \phi < 2\pi$) and pseudorapidity coverage of $|\eta| < 1.1$.

The sPHENIX EMCal is designed to precisely measure photons, electrons and positrons via electromagnetic showers. To achieve this goal, the EMCal has a depth of 18 radiation lengths and its electromagnetic shower resolution was measured in beam tests to be $2.8\% \oplus 15.5\%/\sqrt{E}$ for electrons [8, 9]. The EMCal is also nearly one nuclear interaction length in depth and therefore sees a substantial amount of energy in the ion collisions from hadronic showers as well. The sPHENIX EMCal is a compact sampling calorimeter; it is located just outside of the TPC/TPOT



(a) EMCAL Sector Schematic

(b) OHCal Sector Schematic

Figure 2.8: (a) Schematic of EMCAL sector highlighting projective geometry of towers in η and lightguides and electronics on the inner radius of the sector. (b) Schematic of OHCal half-sector highlighting projective geometry of towers in η , layered absorber/scintillator tile tower design, wavelength-shifting fiber located within HCal scintillating tiles, and readout electronics on the outer radius of the sector. Reproduced from [5].

with an inner radius of 90 cm and the EMCAL and IHCal combined are constrained to fit within the repurposed Babar magnet. The EMCAL uses a tungsten powder absorber, which has a small Moliere radius and large particle stopping power. This allows the EMCAL to have a large number of radiation lengths and precision position resolution while still being compact. Scintillating fibers embedded within the tungsten powder collect and transmit light to a lightguide on the front of each EMCAL block (size 2x2 towers). Following collection by the lightguide, the signals are processed by Silicon Photomultipliers (SiPMs), which convert the light to electric current, and passed through a pre-amplifier. The analog voltage signals are then passed to the Analog-Digital Converters as the start of the sPHENIX calorimeter data acquisition system. The EMCAL is composed of 64 sectors, 2 sectors in η and 32 sectors in ϕ , with each sector containing 384 towers for a total of 24,576 EMCAL towers of tower size $\Delta\eta \times \Delta\phi = 0.024 \times 0.024$. Each sector has six interface boards used to communicate with the detector for setting and monitoring the detector state, including information about the SiPM temperatures, bias voltage and offsets supplied to the SiPMs, leakage current, and detector gain. These slow control communication boards are also used for detector commissioning tasks such as turning on and pulsing LED and test pulses for calibration runs.

The sPHENIX HCal system is the first central barrel hadronic calorimeter on a detector at RHIC and allows for full jet reconstruction with both electromagnetic and hadronic calorimetry at

RHIC energies for the first time. sPHENIX is designed to measure hadronic showers with the full calorimeter system totaling a depth of 5 nuclear interaction lengths and having a hadron resolution response in beam tests of $13.5\% \oplus 64.9\%/\sqrt{E}$ [9]. The HCal system is split into two layers, the IHCAL and OHCal, separated by the Babar superconducting magnet repurposed for sPHENIX. The IHCAL is located between the EMCAL and the magnet with an inner radius of ??? cm and the OHCal is located outside of the magnet acting as the magnet flux return with an inner radius of ??? cm and an outer radius of ??? cm. The IHCAL (OHCal) are sampling calorimeters composed of aluminum (steel) absorber plates and 4 (5) scintillating tiles set at an angle offset to the transverse direction to reduce the amount of collision particles that do not interact with the active volumes of these calorimeters. Wavelength shifting fibers are embedded within the scintillating tiles which collect and transmit the produced light to SiPMs. The SiPMs process this light into voltage signals which is then amplified and digitized in the same manner as for the EMCAL. Both the IHCAL and OHCal contain 32 sectors split into North and South half-sector sides and each sector contains 48 towers for a total of 1536 towers of tower size $\Delta\eta \times \Delta\phi = 0.01 \times 0.01$. Each half sector has one interface and slow control communication board and these are also used to set and monitor the detector state including SiPM temperatures, bias voltages and offsets, leakage current and detector gain.

2.2.3 sPHENIX Global Detectors

sPHENIX contains several global detectors used to provide minimum bias event triggering and total event characterization information such as the vertex of the collision event and centrality of the event. These detectors include the Minimum Bias Detector (MBD), Zero Degree Calorimeters (ZDCs) and sPHENIX Event Plane Detector (sEPD).

The MBD is located at forward rapidity, $3.51 < |\eta| < 4.61$, on both the north and south side of the interaction point, close to the beam pipe, and is repurposed from the PHENIX Beam Beam Counter (BBC) with updated trigger and readout electronics, where it was located in a different position $3.0 < |\eta| < 3.9$ along the beam line [10, 11]. Each side of the MBD contains a set of 64 1-in diameter mesh-dynode photomultiplier tubes (PMT) and the front of these PMTs are connected

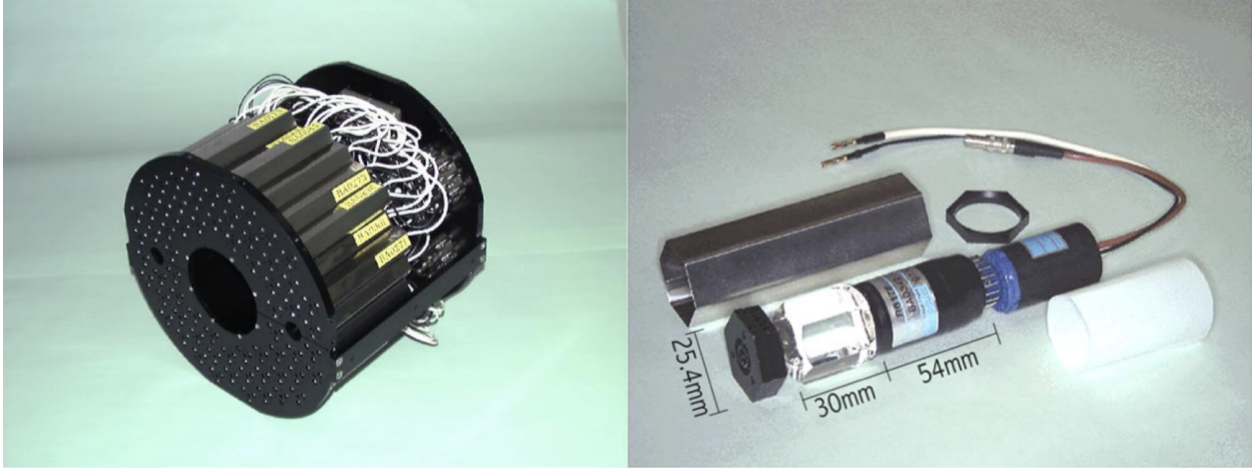


Figure 2.9: Left: Schematic of 64 MBD module array mounted on detector frame. Right: Photo of individual MBD module with quartz radiator and PMT. Reproduced from [5].

with a 3 cm quartz Cherenkov radiator to detect charged particles via Cherenkov radiation. During both PHENIX and sPHENIX running, the MBD has been located close to the beam pipe and is subject to high levels of radiation during data taking. In its original design, quartz was selected for the radiator material and PMTs for signal amplification due to their radiation hardness and over the data taking lifetime of the MBD, the subsystem has not seen any significant degradation due to radiation damage. The MBD is used for online triggering of hadronic interactions and offline to provide a selection of minimum-bias (MB) events and centrality determination in heavy-ion collisions. It is also used for the offline reconstruction of the collision z-vertex position using the arrival time difference between the first charged particles detected by the PMTs on the north and south side of the interaction point.

The ZDCs [12] are located on both sides of the interaction point at very forward rapidity, 18 m from the interaction point, and are also repurposed from the PHENIX detector. They are sampling hadronic calorimeters composed of three modules made of tungsten alloy and PMMA optical fiber with a total of 5.1 nuclear interaction lengths (149 radiation lengths). Utilizing their very forward location, the ZDCs are able to detect beam fragment neutrons of the collision without additional backgrounds from produced particles and secondaries from the collision. A schematic showing how the sPHENIX ZDC detector measures these beam fragment neutrons while not being sensitive

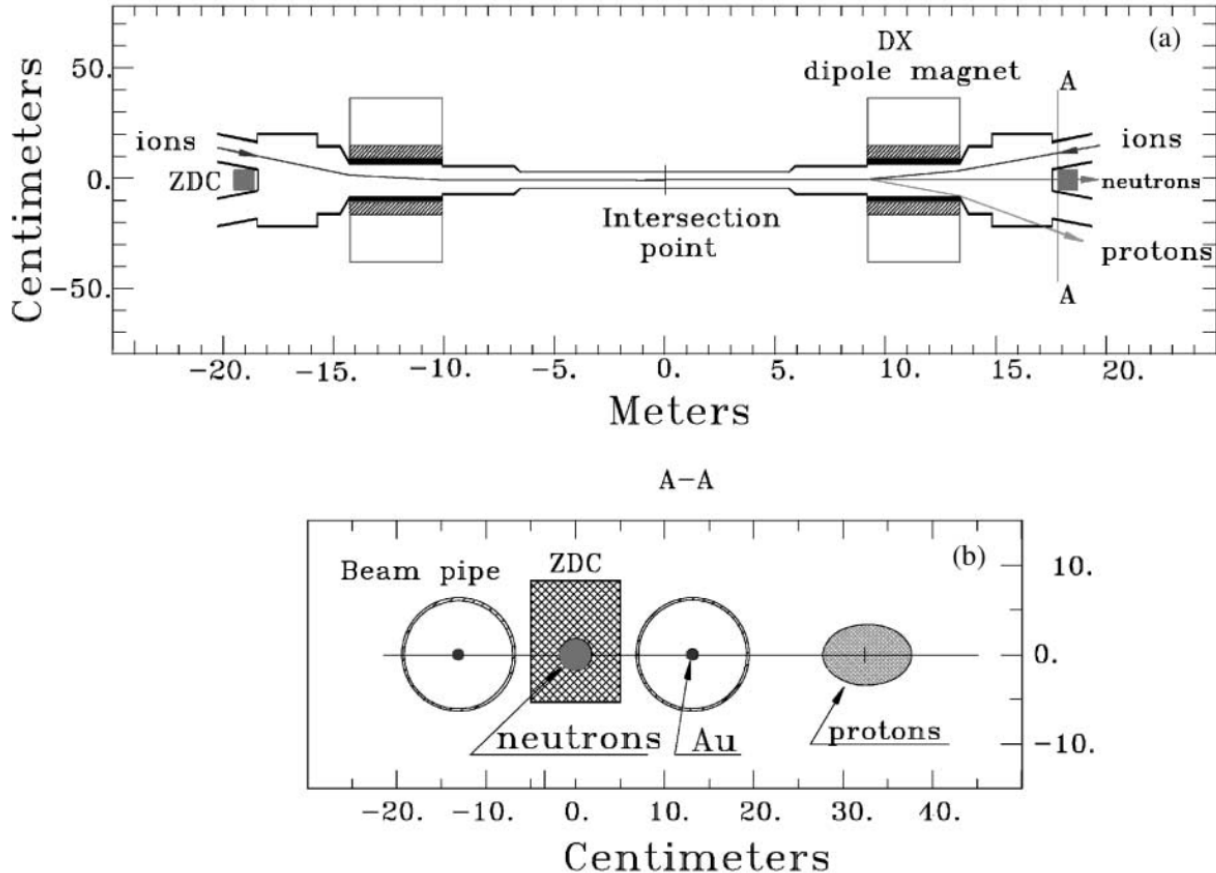


Figure 2.10: Schematic of sPHENIX ZDC detector shown from (a) collision region view and (b) "beam's eye" view to show the ZDC location past the RHIC DX dipole magnets and between the beam pipes. Also shown is the trajectory of beam fragments with neutrons measured in the region of the ZDC and protons deflected. Reproduced from [12].

to beam fragment charged particles can be found in Fig. 2.10. The total energy of the neutrons are measured in the ZDCs via the transmission of Cherenkov radiation from the neutron's hadronic showers by PMMA fibers to PMTs. Each side of the ZDC is calibrated by requiring that the peak in the measured energy distribution which corresponds to the energy deposition of a single neutron is set at the nominal beam energy value of 100 GeV. Additionally, specifically in sPHENIX, criteria on signals in both sides of the ZDC are included in the minimum bias event selection to separate hadronic interactions from beam backgrounds like beam-gas interactions.

2.2.4 sPHENIX Data Acquisition and Readout

sPHENIX is designed with a state of the art data acquisition system and computing resources to collect data at very high rates which is necessary to achieve its data-intensive physics goals within its short three year running period. The sPHENIX data acquisition system is designed to readout data from triggered calorimeter events at a rate of 15 kHz in both p+p and Au+Au collisions and read out tracking detectors in full streaming mode collecting all of the supplied collision data. With the high collision rate ($\gg 15$ kHz) supplied by RHIC, the sPHENIX trigger system is used to make decisions using information from the calorimeter and global detectors on whether to read out a particular collision event. This trigger system uses calorimeter information to identify and save likely high p_T photon and jet events and uses the global detectors to identify and save minimum bias hadronic collision events.

The triggered calorimeter and global detector data is read out by going through in five steps: first the front end modules (FEM) which digitize the analog signals from the SiPMs and PMTs in the detectors, second the data collection modules (DCMs) which combine data from multiple FEMs and act as very short term buffers, the data is then passed through the sub event buffer (SEB) computers used to store the data temporarily, and then is transferred to bufferboxes, before finally being written to disk storage. The tracking data is read out from the front end electronics (FEEs) through the ATLAS "FELIX" card which is connected directly to a standard computer which serves as a buffer similar to the triggered SEBs. The tracking data is also transferred to bufferboxes and written to disk storage in the same manner as the triggered data.

The Really Cool Data Acquisition (RCDAQ) system is used to control and coordinate the entire sPHENIX data acquisition and readout process. The RCDAQ coordinates the start and stop of all of sPHENIX's independent read out data streams and transmission of data of variable types with fixed packet sizes through the different stages of buffer computers. This is necessary to ensure that all subsystems are synchronized in their read out and is especially important since in sPHENIX all subsystem components have independent data stream read out and there is no online event building. Via the transmission of data packets with fixed sizes, the RCDAQ is also able develop a controlled

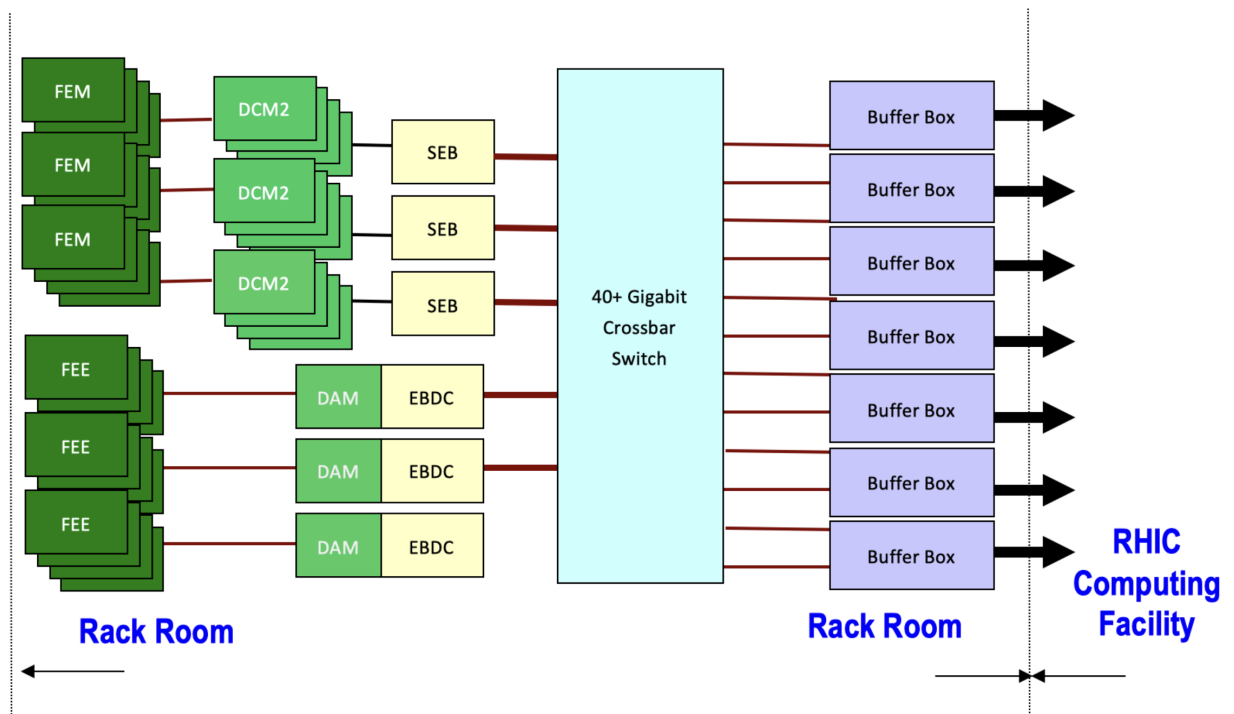


Figure 2.11: Flowchart of sPHENIX data acquisition system showing propagation through the stages of data acquisition from the front end electronics to the RHIC computing facility. Reproduced from [5].

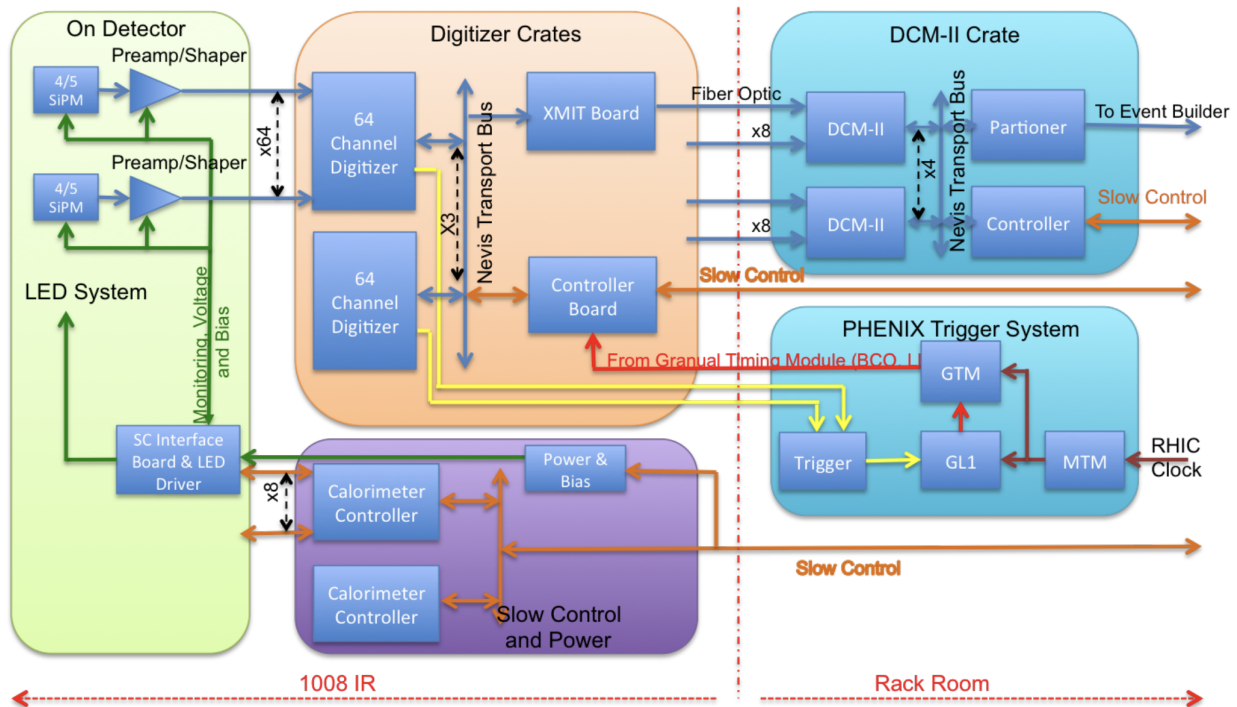


Figure 2.12: Detailed flowchart of sPHENIX data aquisition system for triggered subsystems (calorimeters and global detectors) including feedback on data readout from Trigger System. Reproduced from [5].

and steady flow for the data through the read out system.

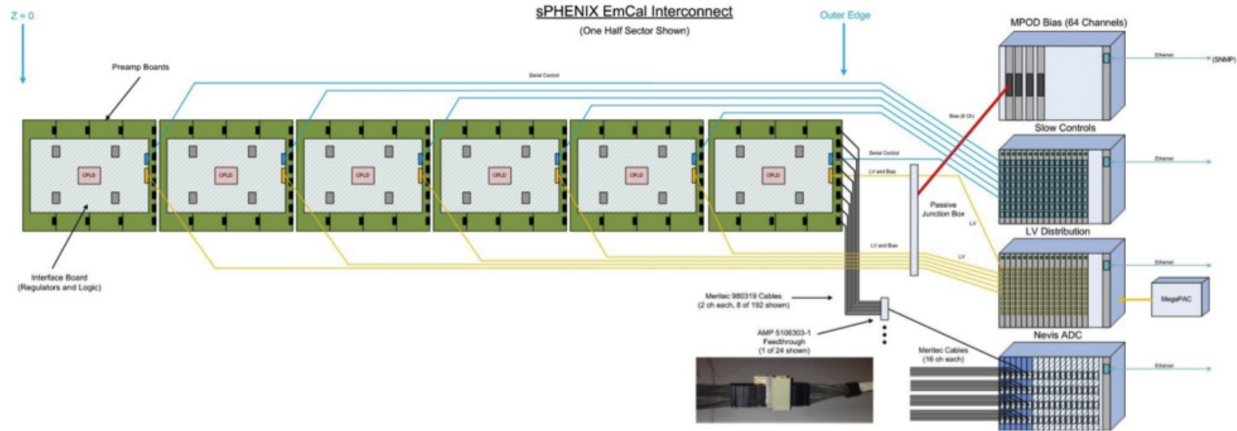
Chapter 3: sPHENIX Calorimeter Commissioning, Reconstruction and Calibration

Substantial work on the calorimeter commissioning, reconstruction, and calibration was necessary before producing high-quality physics results using the sPHENIX calorimeters. This commissioning work included devising and implementing real-time monitoring and logging of the calorimeter detector state and investigating various reconstruction issues in the calorimeter data related to read out electronics issues. Additionally, a vast array of calorimeter calibrations were also necessary to accurately reconstruction the correct energy scale of the calorimeter signals.

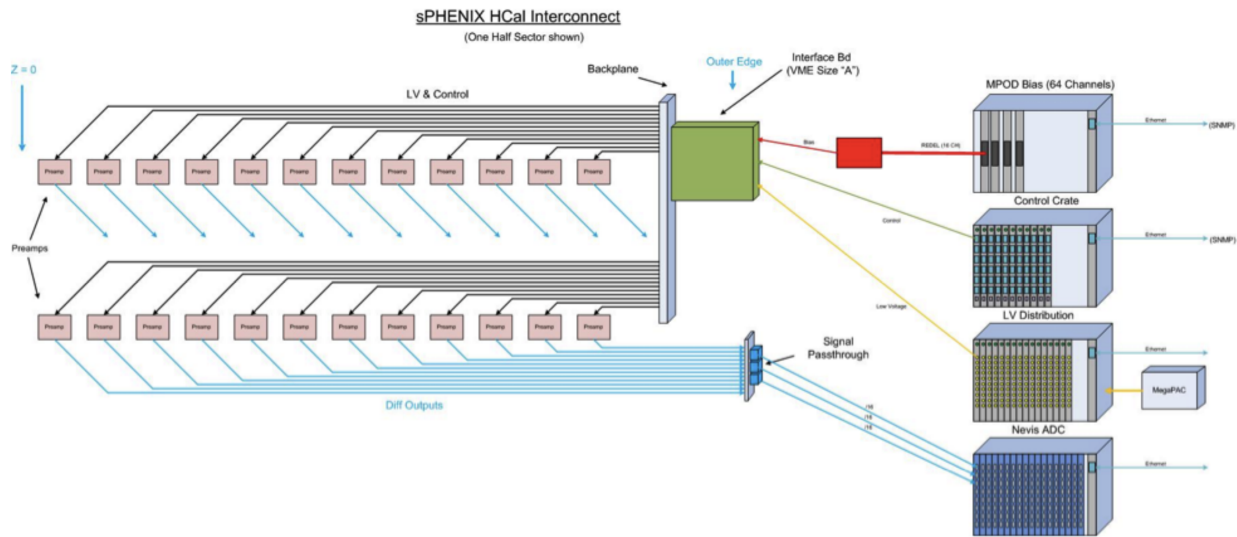
3.1 Real-time Calorimeter State Logging and Monitoring

Each EMCal sector has six interface boards used to communicate with the detector for setting and monitoring the detector state. Each interface board is connected to a slow control communication board, a Multi-channel Power Output Device (MPOD), a low voltage power supply, and an Analog-to-Digital Converter (ADC) board. The slow control communication board is used to set the detector state including information about the SiPM temperatures, set value for the low and bias voltage, tower by tower bias voltage offsets supplied to the SiPMs, tower by tower leakage current from the SiPMs, and pre-amplifier gain mode. These slow control communication boards are also used for detector commissioning tasks such as turning on and pulsing LED and test pulses for calibration runs. A similar control scheme is used for communication with the IHCAL and OHCAL. Here each IHCAL and OHCAL half sector has one interface and slow control communication board and these are also used to set and monitor the detector state including SiPM temperatures, bias voltages and offsets, leakage current and pre-amplifier gain mode.

This information about the detector state is vital both during the online operation of the detector



(a) EMCal Sector Communication Design



(b) IHCAL/OHCAL Half-Sector Communication Design

Figure 3.1: (a) Diagram of EMCal sector design with interface board connections to slow control, MPOD, low voltage power and ADC boards. (b) Diagram of HCal half-sector design with interface board connections to slow control, MPOD, low voltage power and ADC boards. Reproduced from [5]

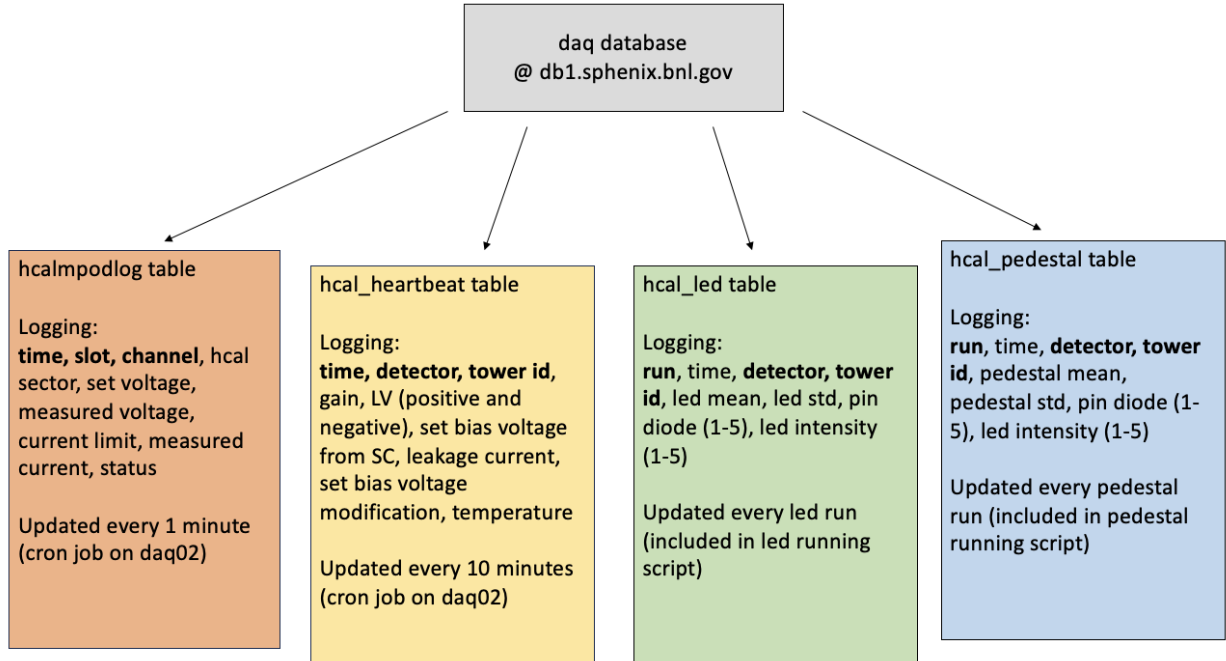


Figure 3.2: Diagram of HCal database table schema for logging detector state information. Includes tables for hcal slow control and bias voltage information as well as LED and pedestal run analysis results.

and during offline reconstruction and calibration of the data. The detector state information for both the EMCAL and HCal is logged in real time by first communicating with the slow control communication boards via a telnet connection, parsing the response, and then writing the detector state information to a PostgreSQL database. The detector state information has been logged up to every 10 minutes for the last three years of data taking.

To accurately map the detector state information into a useable format for reconstruction and calibration, the detector information is keyed on the offline tower id and timestamp of the log entry. This allows for easy access to the tower by tower information for use in calibration tasks such as applying corrections to the HCal absolute energy calibration due to changes in SiPM operating temperature over periods of data taking.

The detector state information is also used to monitor the well-being of the detector in real time. Grafana dashboards, which provide an aggregate view of the logged detector state information, are used by data taking shifters to monitor well-being of the detector in real time. In order to present

clear descriptions of the detector state, the tower by tower information stored in the database is queried and then aggregated to present the overall health of individual sectors or half-sectors of the calorimeters. These dashboards include both real time and time series information on the SiPM and pre-amplifier temperatures, the bias voltages, whether the tower by tower bias voltage offsets are set to their nominal values, and gain modes.

3.2 sPHENIX Low-Level Data Reconstruction

Small introduction to ADC.

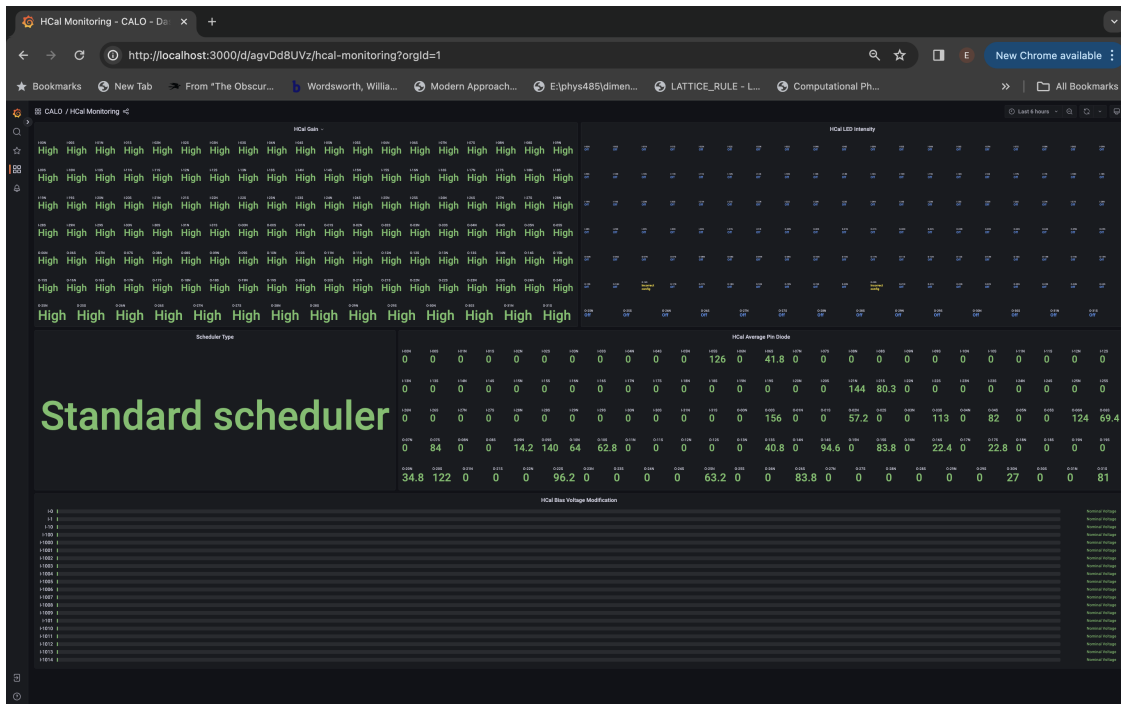
3.2.1 Diagnosing ADC Bit Issues

3.2.2 Online ADC Firmware Fixes

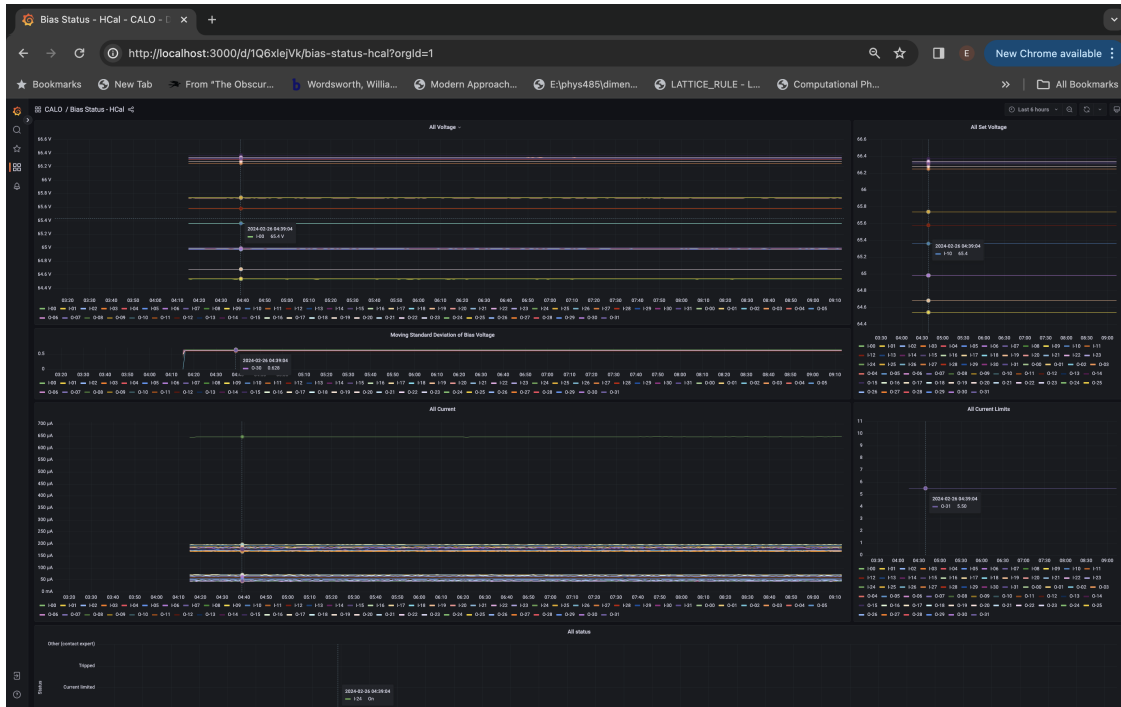
3.2.3 Offline Reconstruction Software Fixes

A small fraction (<0.1%) of the ADC channels in the sPHENIX calorimeters were determined to have intermittent stuck bits due to hardware issues with the ADCs. In the default calorimeter reconstruction chain, waveforms from channels with stuck bit issues were masked as energy contributions from towers with high value stuck bits can easily pollute a physics measurement especially studies of rare high-energy jet and photon measurements. This masking was determined by fitting the waveform to a template and masking based on the value of a quality parameter defined as the least squared error over the number of degrees of freedom of the fit. In this default reconstruction chain, waveforms with stuck bit issues have a characteristic high quality parameter (denoted as χ^2) of 10 times the nominal value range.

While this masking was effective, in an effort to maximize calorimeter acceptance and minimize event-by-event changes in the calorimeter acceptance, a recovery scheme at the offline waveform fitting stage was devised to "un-flip" the stuck bits and recover a high quality, useable waveform. The goal of this recovery method was fairly constrained as to not introduce any reconstruction artifacts into the calorimeter reconstruction chain. Therefore, the recovery method focused on



(a) Shifter Monitoring Dashboard



(b) Bias Voltage Monitoring Dashboard

Figure 3.3: (a) Shifter monitoring dashboard for HCal gain, SiPM temperature and bias voltage offsets, LED and Pin Diode status. (b) Bias voltage monitoring dashboard showing the bias voltage for sector of the HCal.

sPHENIX ADC Module Block Diagram

RHIC beam clock 9.6MHz

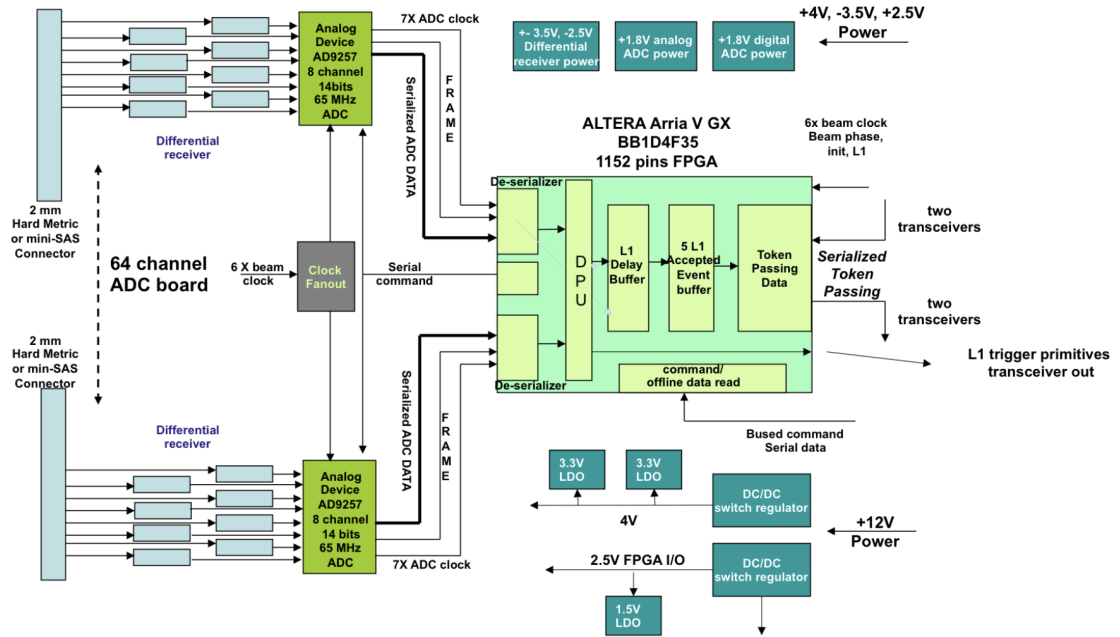


Figure 3.4: Diagram of the ADC board design used for digitization of signals from the sPHENIX calorimeters.

a set of abnormal waveforms where we have a good understanding of the underlying waveform shape and can comfortably do a recovery. The constrained goal was to recover as many single sample bit flip waveforms as possible from waveforms with characteristic high value (bits 2^{11} to 2^{13}) stuck bit behavior which have been previously successfully identified using high χ^2 signature from the template fit. Within this goal was also to reject performing this recovery procedure on other sources of failure that could cause poor waveform fit quality include channels with the previously mentioned shifted bit-stream, waveforms with abnormal shape, and waveforms with lower value stuck bits (bits 2^{10} and below).

The recovery method is defined below and described using psuedocode in Figure 3.5. First, possible stuck bit waveform candidates are identified using the fit quality (χ^2) and pedestal values return from the waveform's fit to the default calorimeter template. Next, a recovery step is performed on these waveform candidates by iterating through bits 2^{11} to 2^{13} and subtracting this bit value if the waveform sample value is greater than the bit value and the subtracted value is greater

```

if (chi2min > _chi2threshold && f->GetParameter(2) < _bfr_highpedestalthreshold && _dobitfliprecovery) {
    std::vector<float> rv;
    for (int i = 0; i < size1; i++) {
        rv.push_back(v.at(i));
    }
    int bits[3] = {8192,4096,2048};
    for (int b = 0; b < 3; b++) {
        for (int i = 0; i < size1; i++) {
            if ((int(rv.at(i)) % bits[b] != int(rv.at(i)) && int(rv.at(i)) % bits[b] > _bfr_lowpedestalthreshold) {
                rv.at(i) = rv.at(i) - bits[b];
            }
        }
    }
    /* rerun template fit method */
    if (recover_chi2min < _chi2lowthreshold) { } Check if new fit chi2 is good using same chi2 threshold as isBadChi2 status
    /* replace waveform with temporary waveform and push new fit parameters + recovered status back to TowerBuilder */
} else {
    /* use original waveform and old fit parameters + not recovered status back to TowerBuilder */
}
}

```

Create temporary waveform vector for recovery

Iterate through bits 2^{11} - 2^{13} and each time sample of the waveform

Check if ADC is above high bit value as well as if subtracting this high bit value would give a value greater than pedestal value, if so do bit subtraction

Check if new fit chi2 is good using same chi2 threshold as isBadChi2 status

Figure 3.5: Pseudo-code algorithm for discovering and recovering calorimeter waveforms digitized with stuck high value bits using the quality of fit to the calorimeter waveform template.

than the waveform pedestal value. Following this bit subtraction, the waveform is refit to the calorimeter template and the quality of the fit is re-evaluated. A example of successful execution of this recovery method for a stuck bit 2^{11} is shown in Figure 3.6.

Channels with shifted bit streams are eliminated from the recovery procedure by requiring that the pedestal calculated from the first round of template fit be < 4000 ADC; these shifted bit stream waveforms have pedestals between 8000 and 10000 ADC while range of normal calorimeter pedestal values are between 1300 and 2000 ADC. Further, channels with very noisy behavior

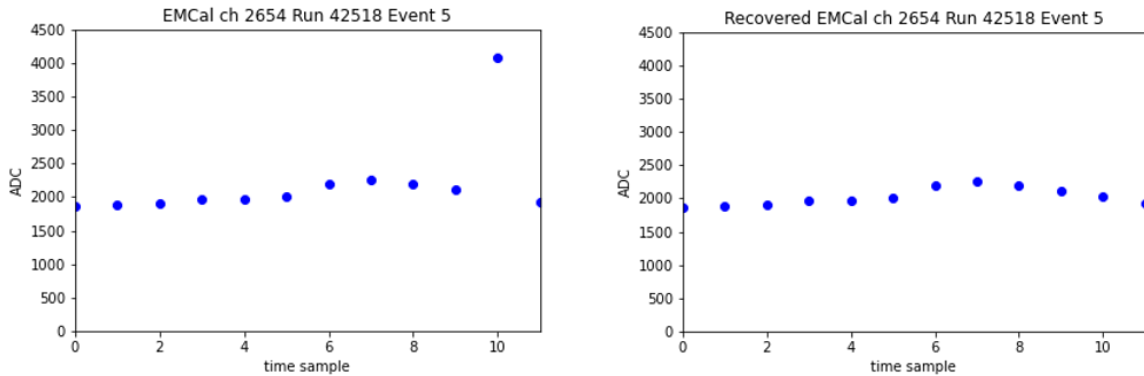


Figure 3.6: Example waveforms of before (left) and after (right) the waveform recovery method for an EMCal channel with a known intermittent stuck bit.

or lower value stuck bits are eliminated from the recovery procedure by requiring that the bit subtraction return a value above pedestal values and the recovered waveform have a good fit quality passing the default fit quality criteria.

3.3 sPHENIX Calorimeter Calibration and Reconstruction Routines

3.3.1 Calorimeter Tower Reconstruction

3.3.2 EMCal Energy Calibration

3.3.3 HCal Energy Calibration

Chapter 4: Transverse Energy Density Measurements in Au+Au Collisions

Chapter 5: Underlying Event Measurements in p+p Collisions

Chapter 6: Last Chapter before conclusion

Conclusion or Epilogue

Use this page for your epilogue or conclusion if applicable; please use only one of the titles for this page. Otherwise, you may delete it.

References

- [1] M. Liu *et al.*, *A Monolithic-Active-Pixel-Sensor-based Vertex Detector (MVTX) for the PHENIX Experiment at RHIC*, Proposal submitted to the DOE Office of Science, Web, Feb. 2017.
- [2] H. S. Ko, “Mvtx: A maps vertex tracker for sphenix at rhic,” Mar. 2023, p. 073.
- [3] Z. Shi, *Heavy flavor physics at the sphenix experiment*, 2024. arXiv: 2401.11036 [nucl-ex].
- [4] C. W. Shih, G. Nukazuka, Y. Sugiyama, Y. Akiba, H. En’yo, T. Hachiya, S. Hasegawa, M. Hata, H. Imai, C. M. Kuo, M. Morita, I. Nakagawa, Y. Nakamura, G. Nakano, Y. Namimoto, R. Nouicer, M. Shibata, M. Shimomura, R. Takahama, K. Toho, M. Tsuruta, and M. Watanabe, *Beam test results of the intermediate silicon tracker for sphenix*, 2025. arXiv: 2509.00908 [physics.ins-det].
- [5] sPHENIX Collaboration, “sPHENIX Technical Design Report,” Tech. Rep., 2019.
- [6] H Klest, “Overview and design of the sphenix tpc,” *Journal of Physics: Conference Series*, vol. 1498, no. 1, p. 012 025, Apr. 2020.
- [7] S. Aune *et al.*, “The sPHENIX Micromegas Outer Tracker,” *Nucl. Instrum. Meth. A*, vol. 1066, p. 169 615, 2024. arXiv: 2403.13789 [physics.ins-det].
- [8] C. A. Aidala, S. Altaf, R. Belmont, S. Boose, D. Cacace, M. Connors, E. Desmond, J. Frantz, E. A. Gamez, N. Grau, J. S. Haggerty, A. Hodges, J. Huang, Y. Kim, M. D. Lenz, W. Lenz, N. A. Lewis, E. J. Mannel, J. D. Osborn, D. V. Perepelitsa, M. Phipps, R. Pisani, S. Polizzo, A. Pun, M. L. Purschke, C. Riedl, T. Rinn, A. C. Romero Hernandez, M. Sarsour, Z. Shi, A. M. Sickles, C. Smith, S. Stoll, X. Sun, E. Thorsland, F. Vassalli, X. Wang, and C. L. Woody, “Design and beam test results for the 2-d projective sphenix electromagnetic calorimeter prototype,” *IEEE Transactions on Nuclear Science*, vol. 68, no. 2, pp. 173–181, 2021.
- [9] C. A. Aidala, V. Bailey, S. Beckman, R. Belmont, C. Biggs, J. Blackburn, S. Boose, M. Chiu, M. Connors, E. Desmond, A. Franz, J. S. Haggerty, X. He, M. M. Higdon, J. Huang, K. Kauder, E. Kistenev, J. LaBounty, J. G. Lajoie, M. Lenz, W. Lenz, S. Li, V. R. Loggins, E. J. Mannel, T. Majoros, M. P. McCumber, J. L. Nagle, M. Phipps, C. Pinkenburg, S. Polizzo, C. Pontieri, M. L. Purschke, J. Putschke, M. Sarsour, T. Rinn, R. Ruggiero, A. Sen, A. M. Sickles, M. J. Skoby, J. Smiga, P. Sobel, P. W. Stankus, S. Stoll, A. Sukhanov, E. Thorsland, F. Toldo, R. S. Towell, B. Ujvari, S. Vazquez-Carson, and C. L. Woody, “Design and beam test results for the sphenix electromagnetic and hadronic calorimeter prototypes,” *IEEE Transactions on Nuclear Science*, vol. 65, no. 12, pp. 2901–2919, 2018.

- [10] M. Allen, M. Bennett, M. Bobrek, J. Boissevain, S. Boose, E. Bosze, C. Britton, J. Chang, C. Chi, M. Chiu, R. Conway, R. Cunningham, A. Denisov, A. Deshpande, M. Emery, A. Enokizono, N. Ericson, B. Fox, S.-Y. Fung, P. Giannotti, T. Hachiya, A. Hansen, K. Homma, B. Jacak, D. Jaffe, J. Kang, J. Kapustinsky, S. Kim, Y. Kim, T. Kohama, P. Kroon, W. Lenz, N. Longbotham, M. Musrock, T. Nakamura, H. Ohnishi, S. Ryu, A. Sakaguchi, R. Seto, T. Shiina, M. Simpson, J. Simon-Gillo, W. Sondheim, T. Sugitate, J. Sullivan, H. van Hecke, J. Walker, S. White, P. Willis, and N. Xu, “Phenix inner detectors,” *Nuclear Instruments and Methods in Physics Research Section A: Accelerators, Spectrometers, Detectors and Associated Equipment*, vol. 499, no. 2, pp. 549–559, 2003, The Relativistic Heavy Ion Collider Project: RHIC and its Detectors.
- [11] K. Ikematsu, Y. Iwata, K. Kaimi, M. Kaneta, T. Kohama, N. Maeda, K. Matsukado, H. Ohnishi, K. Ono, A. Sakaguchi, T. Sugitate, Y. Sumi, Y. Takata, M. Tanabe, and A. Yokoro, “A start-timing detector for the collider experiment phenix at rhic-bnl,” *Nuclear Instruments and Methods in Physics Research Section A: Accelerators, Spectrometers, Detectors and Associated Equipment*, vol. 411, no. 2–3, 238–248, Jul. 1998.
- [12] C Adler, A Denisov, E Garcia, M Murray, H Stroebele, and S White, “The rhic zero degree calorimeters,” *Nuclear Instruments and Methods in Physics Research Section A: Accelerators, Spectrometers, Detectors and Associated Equipment*, vol. 470, no. 3, pp. 488–499, 2001.

Appendix A: Experimental Equipment

 Lorem ipsum dolor sit amet, consectetur adipiscing elit, sed do eiusmod tempor incididunt ut labore et dolore magna aliqua. Ut enim ad minim veniam, quis nostrud exercitation ullamco laboris nisi ut aliquip ex ea commodo consequat. Duis aute irure dolor in reprehenderit in voluptate velit esse cillum dolore eu fugiat nulla pariatur. Excepteur sint occaecat cupidatat non proident, sunt in culpa qui officia deserunt mollit anim id est laborum.

Appendix B: Data Processing

 Lorem ipsum dolor sit amet, consectetur adipiscing elit, sed do eiusmod tempor incididunt ut labore et dolore magna aliqua. Ut enim ad minim veniam, quis nostrud exercitation ullamco laboris nisi ut aliquip ex ea commodo consequat. Duis aute irure dolor in reprehenderit in voluptate velit esse cillum dolore eu fugiat nulla pariatur. Excepteur sint occaecat cupidatat non proident, sunt in culpa qui officia deserunt mollit anim id est laborum.